CHAPTER IV

Dynamics of Vorticity Stretching and Breakup of Isolated Viscoelastic Droplets in an Immiscible Viscoelastic Matrix

Thipphaya Cherdhirankorn[a], Wanchai Lerdwijitjarud[a,b],
Anuvat Sirivat[a], and Ronald G. Larson[c]

[a] Petroleum and Petrochemical College, Chulalongkorn University, Bangkok 10330, Thailand

[b] Department of Materials Science and Engineering, Faculty of Engineering and Industrial Technology, Silpakorn University, Nakorn Pathom 73000, Thailand

[c] Department of Chemical Engineering, University of Michigan, Ann Arbor, Michigan 48109, USA

Abstract

Elastic polystyrene (PS) droplets dispersed in an elastic high density polyethylene (HDPE) matrix are observed under a simple shearing flow between two transparent parallel disks. Two different grades of HDPE and of PS are used to formulate two immiscible blends with the same viscosity ratio of unity but different elasticities and elasticity ratios. Rather than deform in the flow direction and break up at a capillary number of near unity, as is the case for Newtonian droplets in a Newtonian medium, the viscoelastic droplets initially deform in the flow direction after startup of steady shear, but then begin reverting to a spherical shape, and, for the more elastic blend, eventually deform in the vorticity direction. With increasing capillary number, the droplet deforms increasingly along the vorticity direction, and above a critical capillary number Ca_c, breakup occurs when two ends of a drop situated on widely separated streamlines with significantly different velocities are displaced from each other under flow. The transition from alignment in the flow direction for Newtonian or slightly elastic droplets to alignment in the vorticity direction for highly elastic droplets can lead to large increases of the critical capillary number for droplet breakup, up to a factor of thirty greater than for Newtonian liquids.

INTRODUCTION

For Newtonian polymer blends in a simple shear flow, the morphology of the minor (or droplet) phase is governed mainly by two dimensionless parameters: the viscosity ratio, i.e., the ratio of droplet viscosity to matrix viscosity; and the capillary number, the ratio of viscous to interfacial forces (Taylor 1932,1934):

$$Ca = \frac{D_o \dot{\gamma} \eta_m}{2\Gamma} \tag{1}$$

where $\dot{\gamma}\eta_m$ is the viscous shear stress, with $\dot{\gamma}$ is the shear rate and η_m the matrix viscosity, D_0 is initial droplet diameter, and Γ is the interfacial tension.

A steady applied shearing flow that is not so fast as to lead to droplet rupture will eventually stretch a droplet into a roughly ellipsoidal steady-state shape, and the steady-state degree of deformation, defined as the deformation parameter Def, is approximately linearly related to the capillary number as (Taylor 1932,1934)

$$Def \equiv \frac{a-b}{a+b} = Ca\frac{19\eta_r + 16}{16\eta_r + 16} \tag{2}$$

where a and b are the lengths of the major and minor axis of the deformed droplet, respectively. Taylor (1934) predicted that the critical point at which the viscous force overcomes the interfacial force leading to droplet breakup occurs at $Ca_c \approx 0.5$ and $Def_c \approx 0.5$ for a steady (or quasi-steady, if the flow rate is very slowly increased) simple shearing flow with a viscosity ratio of around unity. Here, the subscript "c" stands for the critical condition for breakup. These basic predictions have been confirmed and refined in a number of detailed single-droplet experiments (Rumscheid and Mason 1961; Grace 1982; Bentley and Leal 1986; Guido and Villone 1997). However, when the viscosity ratio is higher than four, no breakup can be observed [Grace (1982)]. These results show that for Newtonian fluids, droplet deformation and breakup is strongly influenced by viscosity ratio, a result that emphasizes the importance of controlling this parameter carefully in any attempt to study the effects of other factors, such as viscoelasticity, on droplet deformation and breakup.

The above results were obtained for Newtonian droplets and matrix fluids; however, most polymers are viscoelastic under normal processing conditions, and so elasticity of the droplet and matrix phases should be an important factor affecting the behavior of droplets under a flow field. It has long been noticed, for example, that in blends of viscoelastic polymer melts, the steady-state average droplet size that results from breakup and coalescence of droplets under shear corresponds to a much higher capillary number than is seen in blends of Newtonian liquids at comparable viscosity ratios. Wu (1987) observed, for example, that the steady-state droplet size in extruded viscoelastic polymer blends at a viscosity ratio of unity is around ten times higher than would be obtained for Newtonian components at the same viscosity and at the same shear rate. Lerdwijitjarud *et al.* (2002) found that in blends of 20% polystyrene in polyethylene sheared in a rheometer, the steady-state droplet size corresponded to a capillary number ranging from 2 to 30, depending on the relative magnitudes of the normal stress differences in the droplet and matrix phases and on the viscosity ratio. These capillary numbers are from 4 to 80 times higher than the critical capillary number for breakup of a Newtonian droplet in a Newtonian matrix. While it might be thought that this large increase in droplet size and hence capillary number could be due in part to coalescence effects present in blends, Lerdwijitjarud *et al.* (2003) showed recently that in a 20% blend of a Newtonian liquid in a Newtonian matrix the steady-state capillary number is actually lower than the critical capillary number for breakup of an isolated droplet, i.e., the disturbances to the flow produced by the presence of the other droplets enhances breakup of a given droplet to an extent that more than offsets any increase in droplet size due to coalescence. Thus, the high steady-state capillary numbers observed in blends of viscoelastic polymers must be attributed to the role of viscoelasticity.

Elasticity in the droplet or matrix phase can be quantified by the Weissenberg number Wi, a ratio of elastic to viscous forces, which we here will estimate using either the first normal stress difference N_1 or elastic modulus G' as a measure of the elastic forces and the shear stress as a measure of the viscous forces. Like the capillary number, the Weissenberg number increases with increasing shear rate, since elastic forces generally increase with shear rate more rapidly than do viscous forces. For a given droplet size, Wi and Ca are proportional to each other;

however, since Ca depends on droplet diameter and Wi does not, these two dimensionless numbers can be varied independently by varying both the shear rate and the droplet size for a given pair of viscoelastic fluids. Since both phases can be elastic, there are two Weissenberg numbers, the droplet Weissenberg number Wi_d and the matrix Weissenberg number Wi_m. Since the elastic stresses in the droplet depend on the strength of the flow in the droplet, which is, in turn dependent on the viscosity ratio (more viscous droplets have weaker internal flows), it is clear that in general there is a coupling between the viscosity ratio and the strength of the elastic forces in the droplet. To minimize this influence, in what follows, we will work with fluids having viscosity ratios near unity, and use the macroscopic shear rate to characterize the flow inside the droplet. That is, following the work of Lerdwijitjarud *et al.* (2002), we will not attempt to use the actual flow in the droplet to estimate the droplet Weissenberg number, but will characterize the elasticity of the droplet using Wi_d defined by the droplet fluid properties at the macroscopic shear rate measured on the pure droplet fluid in a rheometer.

Recently, single viscoelastic droplets in Newtonian or viscoelastic matrices have been observed microscopically in simple shearing flows. Lerdwijitjarud *et al.* (2003) observed deformation and breakup of isolated droplets of weakly elastic fluid ($Wi_d \leq 0.02$) in a Newtonian matrix, and found that droplet elasticity produces a slight (up to around 20%) increase in Ca_c, the critical capillary number for droplet breakup. The breakup mechanism appeared to be similar to that in a Newtonian fluid; i.e., the droplet deformed increasingly in the flow direction as the shear rate was gradually increased, until breakup occurred. Elasticity of the droplet produced a reduction in the degree of deformation at any given shear rate and a greater critical deformation at breakup, resulting in a higher Ca_c. However, at the highest Weissenberg number, this effect appeared to be saturating, leading to only a modest increase in Ca_c.

Mighri *et al.* (1998) investigated the influence of elastic properties on droplet deformation and on the critical shear rate, or critical capillary number Ca_c for breakup. The deformed elastic droplet was roughly spheroidal with slightly sharpened edges while a Newtonian droplet retained smooth curved ends. Mighri *et al.* (1998) reported that the degree of droplet deformation, the critical shear rate for breakup, and the breakup time after startup of shearing increased with increasing

elasticity ratio between the droplet and the matrix fluids. They defined the elasticity ratio, k', as the ratio of the Maxwell relaxation time (λ) of the droplet phase to that of the matrix phase, where $\lambda = N_{1i}/2\eta\dot{\gamma}^2$, where N_{1i} is the first normal stress difference. Breakup occurred by an unsteady deformation of the droplet into a thin and long thread, followed by end pinching, and undulations along the droplet surface, finally resulting in a series of alternating large and small (or "satellite") droplets. Moreover, they found that for a low or modest elasticity ratio, $k' \leq 4$, the critical capillary number Ca_c for droplet breakup in steady shearing flow increased with increasing k', reaching $Ca_c \approx 1.75$ at high elasticity ratio, $k' \approx 4$, compared to $Ca_c \approx 0.5$ for Newtonian droplets. Thus, droplet resistance to deformation and breakup increases with increasing elasticity ratio of droplet to matrix phase. While the elasticities of the droplets studied by Mighri *et al.* (1998) were higher than those studied by Lerwijitjarud *et al.* (2003), the droplets in both studies deformed in the flow direction, and the increase in critical capillary number produced by elasticity saturated at a relatively modest values near unity, far below the steady-state values observed in highly viscoelastic polymer blends. These studies, and those described below, suggest that large increases in Ca_c result from a new mode of droplet deformation and breakup for highly elastic droplets.

A new, viscoelastic, mode of droplet deformation, that of droplet extension *in the vorticity direction* (perpendicular to both the shear and shear gradient directions) was apparently first reported for an elastic polymer droplet in a polymer matrix by Bartram *et al.* (1975). An apparently related phenomenon of *widening* of an extended viscoelastic droplet in a highly viscoelastic matrix was later observed by Levitt and Macosko (1996), who suggested that there is a relationship between the second normal stress difference of droplet and matrix phase and the degree of widening. Hobbie and Migler (1999) studied dilute emulsions of viscoelastic droplets in viscoelastic matrices at high shear rate and also observed elongation of the droplet in the vorticity direction at $\dot{\gamma} \sim 280\ s^{-1}$ for viscosity ratio $\eta_r = 1.8$. By extrapolating data at high shear rates to lower rates, they obtained critical capillary numbers for droplet vorticity alignment of around 53, 13, and 11 for viscosity ratios, η_r, of 1.8, 22, and 240, respectively. The increase in critical capillary number for vorticity

alignment with viscosity ratio is consistent with a mechanism involving droplet elasticity, since a higher droplet viscosity would require a higher external flow rate to attain the same internal flow rate within the droplet, which would be needed to maintain a high elasticity of the droplet fluid.

Migler (2000) observed the deformation of highly elastic droplets in a polymeric matrix under a shear flow. The viscosity ratio was near unity, but the elasticity ratio of the droplet to the matrix was higher than 100; that is, the matrix phase was nearly Newtonian under the conditions of the experiments. In a weak shear and for small droplets [Ca < 5], the droplet orientation was found to be along the flow direction, whereas in a strong shear and for large droplets [Ca > 5], the orientation was along the vorticity axis with a broad distribution of aspect ratios.

Mighri and Huneault (2001) studied the deformation and breakup of a single droplet of viscoelastic Boger fluid in a Newtonian matrix, sheared in a transparent Couette flow cell. At low shear rate, they found that the steady-state deformation increased with shear rate as expected, but above a critical shear rate [Ca ~ 5] the deformed drop began contracting in the flow direction and changed its orientation to the vorticity axis. With further increases in shear rate, this elongation in the vorticity direction increased until breakup finally occurred at a capillary number no higher than Ca~35. They proposed that the critical shear stress for reorientation of the droplet in the vorticity direction was probably related to the values of the first and second normal stress differences and their dependencies on shear rate. They also suggested that this reorientation occurred because of a the flow-induced circulatory flow in the droplet that produced an elastic circular hoop stress in the plane containing the shear and the shear gradient directions that squeezed fluid out along the axis perpendicular to this plane, that is, along the vorticity axis. They surmised that in a startup of a steady shearing flow, the deforming viscous stress rapidly reached steady state, but the normal stresses generated by the dispersed phase required a longer time, which caused a gradual increase in droplet elongation along vorticity axis until either a steady-state deformation was reached or breakup occurred. When a droplet was highly stretched in the vorticity direction, they observed small rocking instabilities in the velocity gradient direction causing the two

ends of the droplet to sample significantly different velocities periodically, which ultimately tore apart the droplet into two or more smaller drops.

In our work reported below, we take a further step towards understanding the behavior of commercial blends by using elastic polymer melts for both the droplet phase and the matrix phase. To neutralize any effect of variations in the viscosity ratio, we choose pairs of commercial polymers whose viscosity ratios remain relatively constant near unity when shear rate is varied. Using a flow cell mounted on an optical microscope, we observe the transient deformations of isolated droplets after startup of steady shear flow between parallel disks. By varying droplet size and shear rate, the effects of capillary number and elasticity (or droplet Weissenberg number) are isolated and investigated at fixed viscosity ratio very near unity. Our findings confirm those of Mighri and Huneault, who used nearly Newtonian matrix fluids, but, in addition, we find that when both the droplet fluid and the matrix fluid are highly elastic, droplet deformations during start-up of steady shearing show large oscillations before reaching steady state.

EXPERIMENTS

A. Materials

High density polyethylene and polystyrene (suppliers and grades given in Table 1) were used as matrix and droplet phases, respectively. Both polystyrene grades were obtained from the manufacturers in the form of flake; they were crushed and size-selected by passing the flakes through a 425-mm sieve. To eliminate volatile components, all polymers were heated to around 80°C under vacuum for 12 hours. The polymer blend systems and their experimental temperatures are listed in Table 2.

B. Rheological Characterization

Each polymer was molded into a disk, 25 mm in diameter and 1 mm thick by using a compression mold (Wabash, model V50H-18-CX) at 145°C for HDPE1 and PS1, and at 135°C for HDPE2 and PS2 under a force of 10 tons. We used a cone-and-plate rheometer (Rheometrics Scientific: Model ARES, 25-mm plate diameter with cone angle 0.1 rad) to obtain viscosities and first normal stress differences of the pure polymers. From the rheological properties of pure polymers at various temperatures, the desired pairs of polymers and operating temperatures were selected for further study; and their steady-state viscosities and first normal stress differences as functions of shear rate are shown in Fig. 1 (a) and (b). At low shear rates, the ratio of droplet-to-matrix first normal stress differences N_{1r} of system B could not be precisely determined due to the force-measurement limitations of the rheometer. However, in the low-shear-rate and low-frequency regimes, $N_1(\dot{\gamma})$ is approximately equal to twice G' (ω) at $\dot{\gamma}=\omega$, thus N_{1r} can be estimated by the corresponding ratio of storage moduli, G'_r. The viscosity ratios and G' ratios of the two polymer systems are shown in Fig. 2. In addition, the stabilities of all polymers to thermal degradation were tested at their experimental temperatures by measuring the viscosity at a constant shear rate, 0.5 s^{-1}, for 4 hours; in all cases the viscosity values remain unchanged, allowing us to conduct blend experiments on each system for periods as long as four hours.

C. Observations of an Isolated Droplet in Shearing Flow

1. Shearing Apparatus

To observe the droplet behaviors in simple shearing flow, we used a flow cell (Linkam CSS 450, Linkam Scientific Instruments Ltd., UK) consisting of two transparent quartz parallel disks mounted on an optical microscope (Leica DMRPX, Leica Imaging Systems LTd., Cambridge, England), and connected to a CCD camera (Cohu 4910, Cohu Inc., CA). In addition, the images were analyzed on a computer using the Scion image software.

2. Sample Preparation

HDPE used as the matrix polymer was molded into a disk 25-mm in diameter and 0.5-1 mm thick by compression molding at 145°C for HDPE1 and 135°C for HDPE2. Various PS droplets were introduced into the matrix by using a pin to put a small amount of PS powder on a HDPE disk, and then covering this with another HDPE disk to form a sandwich. The sample was then placed between the top and the bottom disks of the flow cell, both of which were brought into contact with the sample, which was then heated to the testing temperature.

3. Droplet Shape Relaxation Time

We attempted to determine the interfacial tensions by measuring the deformation parameter Def (cf. Eq. 2) of a retracting droplet vs. time, which is known to decay exponentially [Lucinia *et al.* (1997)]:

$$Def = Def_o \exp\left(-\frac{t}{\tau}\right) \tag{3}$$

so that the slope of Def vs. t on a semi-log plot can be related the characteristic relaxation time for a single drop, τ. By equating this characteristic relaxation time to that predicted by the Palierne model (Eq.4) [Palierne (1990) and Graebling *et al.* (1993)], the apparent interfacial tension was then calculated from the following relation

$$\tau = \frac{(3 + 2\eta_r)(16 + 19\eta_r)r_o\eta_{m,o}}{40(1 + \eta_r)\Gamma} \tag{4}$$

To obtain images of the relaxing droplet after a large strain, the desired strain was imposed onto a selected drop in the field of view of the microscope which moved the droplet out of the field of view, then the droplet was left to relax at least 40-50 min (which is equal to or greater than the droplet relaxation time) to ensure that the drop had returned to the spherical shape, and then the droplet was moved back into the field of view by imposing the same strain in the reverse direction. A hundred to 200 images were then recorded (10-20 second per frame) while the droplet relaxed its shape. For both systems, the droplet size was varied from around a hundred micron up to 400 μm or thereabouts. Fig. 3 (a) and (b) shows that the apparent interfacial tension values inferred from Eq. 4 increases with the droplet size. This dependence of apparent interfacial tension on droplet size is likely caused by the contribution of droplet elasticity to the relaxation of the droplet shape. For large enough droplets, relaxation should become slow enough that viscoelastic stresses relax too quickly to influence droplet shape relaxation and hence the rate of relaxation is governed by interfacial tension alone. Thus, the interfacial tension value obtained for large droplets is expected to be the most accurate. Unfortunately, because of the limitation in the ratio of a gap width to an initial droplet size, which was kept at greater than 5, we cannot attain a regime in which the apparent interfacial tension becomes independent of droplet size; see Fig. 3. Therefore, the values of the interfacial tension for the polymer blend systems used in this work were taken from the literature [Brandrup and Immergut (1989)], which are 5.79 mN/m for system A at 147°C, and 5.92 mN/m for system B at 139°C.

From the optical microscope, the droplet images were captured only from the top view, i.e., a view containing the flow and vorticity directions. Since only a projection of the droplet onto the vorticity plane can be imaged from this view, this view cannot determine the true lengths of the principal axes, because two of them (those in the flow and the shear-gradient directions) are not parallel to the vorticity plane. However, the lengths of these axes can be determined by using the affine

angle of rotation of the droplet in the plane containing the flow and shear-gradient directions (Larson 1988) together with the condition of volume preservation, $D_o^3 = abc$ (Almusallam *et al.* 2000).

Although the lengths of the principal axes can be approximated by using the method mentioned above, for convenience we use the lengths of the observable axes, shown in Fig. 4, to describe the behavior of each droplet. Thus, we define a modified deformation parameter Def* as:

$$Def^* \equiv \frac{a^* - c}{a^* + c} \tag{5}$$

where the asterisk denotes that the deformation parameter is an apparent one obtained from the droplet image projected onto the flow-vorticity plane; see Fig. 4.

4. Transient Deformation

The deformed shapes were observed as a function of time from initial to steady-state shapes. Because the Linkham device has one stationary and one moving plate, a single droplet cannot be viewed continuously from startup of shearing to attainment of steady-state shape, since this droplet will pass out of the viewing plane after imposition of around 10 strain units. However, since the behavior of a given isolated droplet is highly reproducible, the strain dependence of the deformation can be determined by combining the results of several experiments. In experiments of type 1, we first move the droplet out of the viewing window by imposing a shearing strain of less than 40 strain units. After allowing the droplet to relax its shape for at least 40 minutes, an observed shear rate was imposed at the same strain but in opposite direction, eventually bringing the droplet back into the viewing window, where it can be observed during deformation. However, the droplet could not be subjected to a large strain in this type of experiment, since this would move the droplet again out of the viewing window. So, to obtain droplet deformation at large strains, we performed experiments of type 2, in which we sheared continuously, and imaged the droplet each time it passed through the viewing window in its orbit around the axis of the rotation of the rotating plate. Typically, one orbit would require around 40 strain units. To get a clear image of the droplet without a high-

speed camera, we stopped the flow briefly each time the droplet reached the center of the viewing image and video recorded its shape over a period of around 1 second, which is a time much too short for the droplet to relax its shape significantly. Then the flow was resumed again until the droplet again reached the viewing window. By repeating the experiment on droplets of similar size, which were stopped at different times, we could assemble a consistent curve from multiple droplets of the droplet deformation versus time at a given shear rate. In the following, the results from different droplets will be presented using different symbols, showing the consistency of results combined from multiple droplets. In each experiment, the time for one revolution of a droplet was recorded with a stopwatch along with the time shown on the Linksys program. To avoid interactions with the plates, the ratio of the gap width to the initial diameter of a selected drop was kept higher than 10, and only droplets near the center of the gap were observed. The experiment was repeated with more than 10 droplets with initial diameters around 75 ($\pm$10%) μm. were used, and the imposed shear rate was 0.5 s^{-1}. Similar experiments (only type 2) were carried out using other droplet sizes, 52, 110 and 120 μm, but the same shear rate of 0.5 s^{-1}. To separate the effect of shear rate from that of elasticity, another set of experiments were carried out on droplets of different sizes [135, 75, and 46 μm] but in which the shear rate varied inversely with droplet size from 0.28, to 0.5, to 0.8 s^{-1}, In this way we could vary the viscoelastic forces, which increase with increasing shear rate, while holding the capillary number fixed at around 8 by varying the droplet size inversely with the shear rate.

5. Steady-State Deformation and Breakup

From the transient experiments, the required strain to reach steady state can be determined and was found to be around 2500 strain units. To determine the steady-state droplet shape as a function of capillary number, we carried out experiments up to high strains at two different shear rates and for different droplet sizes. The selected shear rates were 0.3 and 0.5 s^{-1} for system A, and 1 s^{-1} for system B, which are high enough that the needed strain could be achieved within an

acceptable time, but not so high that the steady-state droplet shapes are too small to be imaged clearly. In addition to using these two shear rates, different droplet sizes were chosen to vary the capillary number at fixed elasticity. After loading a sample, droplets were allowed to relax to spherical shapes for a period of at least 50 minutes, a bit longer than for the transient experiments described earlier, since some of the droplets used were larger and so needed somewhat longer to relax. A constant shear rate was then applied until a strain exceeding 2500 strain units had accumulated. When a selected droplet passed through the viewing window, the motor was stopped for less than a second and a video movie (speed 25-fps) was then recorded, as described earlier in the description of the experiments measuring transient droplet shapes. To ensure that the steady state deformation had indeed been attained, we repeated imaging the same droplet for several more passes of the droplet through the viewing window over a period of 5 to 10 min. In addition, after turning off the flow the droplet shape relaxation was recorded at a videorecording speed of 10-20 seconds per frame for approximately 1 hour.

When the droplet size was varied at fixed shearing rate, we found a critical droplet size above which no steady state-shape was obtained. For these droplets, the unstable shape of the droplet was recorded with time, by imaging the droplet each time it passed through the viewing window (as in the experiments discussed earlier), until the droplet broke.

RESULTS AND DISCUSSION

A. Deformation in Steady Shear Flow

1. Observations of Droplet Deformation

We first consider system A, in which both matrix and droplet phases are highly elastic with a G' ratio of 0.7 at ω = 0.5 rad/s. A shear rate of 0.5 s^{-1} and a droplet size of 75 ($\pm$10%) μm were selected for study at a well-controlled temperature (147°C). We observed that the shape of the deformed drop, Def*, under steady shear flow oscillates before attaining a steady state shape, as shown in Figs. 5 and 6. We divide the transient deformation into 5 regimes. In the first regime, a*, the principle axis projected in the flow direction, shown in Fig. 5 (c), oscillates with a periodicity of around 10 sec, while c, the length of the principle axis in the vorticity direction, shown in Fig. 5 (d), does not change from its initial value until near the end of regime 1. From the absence of a variation in c, we infer that this oscillation may arise from a droplet tilting or rotation around the vorticity (z) axis as shown schematically in Fig. 7. Eventually, near the end of regime 1, while it is still tilting or rotating, the droplet begins to contract in the z-θ plane, and the c axis increases slowly. In the second regime, the drop gradually elongates in the vorticity direction, and after around 500 sec (or 250 strain units) elongation in the vorticity direction reaches its maximum at the end of this regime. At the maximum |Def*| between the regime 2 and 3, as shown in Fig.5 (a), the c axis is much larger than its initial value so that $c/D_o \sim 1.35$, while the a axis returns to a length nearly equal to its initial value [Fig. 5 (c)]. From volume conservation, this implies that the droplet is flattened in the z direction, as shown in Fig. 8. However, the deformed drop is not stable at this point because in regime 3, the droplet rapidly contracts in the vorticity direction; see Fig. 5 (d). While contracting in the vorticity direction and stretching occur along the flow direction, cusps emerge out of each side of the droplet along the vorticity axis, as can be seen in Figs. 6 (k) and (l). After 1000 strain units have been imposed, the droplet stretches in the vorticity direction again (regime 4) until a steady-state shape is attained at around 2000 strain units in the fifth regime, as shown in Fig. 5 (b).

These phenomena do not occur in system B, whose droplet and matrix phase elasticities are both lower than in system A, but whose elasticity ratio of droplet to matrix phase is higher than in system A, as shown in Figs. 1 and 2. When a constant shear rate of 0.4 s^{-1} is applied to system B, the deformation parameter rises rapidly from zero to around 0.09, and then slowly and roughly exponentially decreases with time until attaining a steady-state value shown in Fig. 9. This finding is similar to that of Mighri and Huneault (2001) who reported that under a strong shearing flow, an elastic droplet in a Newtonian matrix rapidly stretches along the flow direction, and then gradually contracts in this direction after the first normal stress difference in the droplet has developed sufficiently. Our Fig. 9 is very similar to Fig. 7a of Mighri and Huneault, except that in the latter, the droplet eventually becomes aligned in the vorticity rather than in the shear direction; i.e., the deformation parameter becomes negative. We also obtain negative steady-state values of Def* for system B at higher values of Ca (as will be presented below). The similarity between our results for system B in a torsional plate-plate flow and the results of Mighri and Huneault in a circular Couette flow implies that the unusual oscillatory droplet deformation we observe for system A is not an artifact of our system geometry. We speculate that the oscillations arise only in blends for which both phases are highly elastic, and occur because the different growth periods for the first normal stress differences of the two phases produce time-delayed imbalances in the normal stress conditions on the droplet surface.

2. Effect of Ca on Droplet Deformation.

In this section, the elasticity of the droplet and matrix phases are held constant by holding the shear rate fixed at 0.5 s^{-1}. At this shear rate, where the G' ratio for blend A at ω = 0.5 rad/s is 0.7, we selected various initial droplet sizes to vary the capillary number at a fixed droplet/matrix elasticity ratio. The deformation parameter Def* vs. time from the 2^{nd} to 5^{th} regimes of the 52, 79,110 and 120 μm-drops is shown in Fig. 10 (a). It can be seen in Fig. 10 (b) that between the second and the fourth regimes, droplets with higher Ca show a greater deformation in the flow direction (larger a^*/D_o). However, for all Ca values in these experiments, nearly

the same value of c/D_o is reached at its minimum point at the boundary between regimes 3 and 4, as shown in Fig. 10 (c). For Ca values of 5 and 8, steady shapes are attained at strains around 1300 and 2000 (times of 2600 and 4000 seconds), respectively, with larger droplet deformations (more negative Def*) occurring with increasing capillary number. The larger droplets with diameters of 110 and 120 μm (higher capillary numbers of 11 and 12), do not attain steady-state shapes. For these droplets, the vorticity axis, c, rapidly increases for a long period and the axis in the flow direction (a*) slightly decreases until the drops eventually break [Fig. 10 (b) and (c)].

3. Effect of Elasticity on Droplet Deformation

To investigate the effect of elasticity in system A, the capillary number was kept constant at 8 and the shear rate and drop size were varied inversely with respect to each other. Shear rates of 0.28, 0.5, and 0.8 s^{-1} were chosen and the droplet sizes used for these shear rates were 135 (2 runs), 70-79 (repeated experiments), and 45 μm, respectively. Fig. 11 (a) shows that there is a significant decrease in the maximum value of Def^* vs. t (at a strain of around 900) as the shear rate (and hence the elasticity) increases. As shown in Figs. 11 (b) and (c), this decrease results mainly from a decrease in a^*/D_o, rather than an increase in c/D_o. The steady-state value of Def* in regime five is nearly the same for all shear rates.

B. Steady-State Deformation and Droplet Breakup Mechanism

The strains required to attain steady state at each shear rate were determined at shear rates of 0.3 and 0.5 s^{-1} for system A, and at 1 s^{-1} for system B. By increasing the droplet size, the capillary number was varied. As shown in Fig. 12, when Ca increases, the steady-state deformation *in the vorticity direction* increases; i.e., Def^* becomes more negative. This contrasts with the behavior of a Newtonian system where the steady-state deformation *in the flow direction* increases *monotonically* with Ca [Taylor (1934), Tsakalos *et al.* (1998), Guido and Villone (1998)]. Fig. 12 shows that a droplet in both systems starts to stretch in the vorticity direction at Ca

around 3. Whereas Mighri and Huneault (2001), using less viscous liquids, found that at Ca less than 10, an elastic droplet in a Newtonian matrix deforms along the flow direction with steady-state deformation increasing with increasing Ca, until Ca reaches roughly 5, above which the droplet starts contracting in the flow direction. At each value of Ca a droplet in our system B deforms less in the vorticity direction than one in system A (lower |Def*|; see Fig. 12). This might be the result of the generally lower elasticity of system B. At the shear rate of 0.5 s^{-1} in system A, for droplets larger than 92 μm do not attain a steady shape, but the droplet eventually breaks up (see Section part A2 above); this size corresponds to a critical value of Ca for breakup of around 9, where the corresponding value of Def^*_c is around -0.27. In addition, the critical capillary number of system A is somewhat comparable to the steady state critical Ca, which was around 6, in Lerdwijitjarud *et al.* (2002). Their system, PS(drop)/HDPE(matrix), like ours, had a viscosity ratio of unity and an N_1 ratio of around 0.7. A droplet in system B breaks at a higher value of Ca (greater than 14) than for system A (around 9). At the viscosity ratio of unity and N_1 ratio of 2, the steady state critical Ca was found to be around 12 in Lerdwijitjarud (2002). This is slightly less than the approximately Ca_c in ours (for system B). As shown in Fig. 2, the elasticity ratio (G'_r at the selected shear rate) of system B is 3-4 times higher than that of system A, which might account for the difference in critical capillary numbers for systems A and B. An alternative explanation might be that the weaker elasticity of system B produces less deformation in the vorticity direction than for system A at the same capillary number, and hence a greater shear rate is needed to stretch droplets in system B sufficiently to produce rupture. If this latter explanation is correct, then droplets with intermediate elasticity, high enough to avoid elongation in the flow direction, but low enough to avoid large elongations in the vorticity direction, will be most resistant to rupture and will break at the highest capillary number.

In our more elastic blend A, when a constant shear rate above Ca_c is applied, a spherical drop deforms non-monotonically until regime five is reached and the droplet then elongates continuously in the vorticity direction until breakup occurs as shown in Figs. 10 (a), (b), and (c). The droplet breaks when its two ends are quite far apart and no longer located on nearby streamlines, as shown in Fig. 13. Mighri and

Huneault (2001) found that in a counter-rotating circular Couette cell, a viscoelastic droplet breaks when its two ends separated along the vorticity direction develop unstable motions because of large velocity differences between the two moving layers. A similar instability may occur in our flow, but it is less visible, since we view the droplet along the shear gradient direction, rather than along the vorticity direction as Mighri and Huneault did.

We note that we could find no clear correlation in the literature or our data between droplet Weissenberg number and re-orientation or break-up. The effect of elasticity may involve a complicated interplay of the first and second normal stress differences of both phases, and may couple to viscosity ratio, shear thinning, and capillary number. Careful experiments in which all these quantities are carefully controlled, along with numerical simulations of viscoelastic droplet deformation and breakup will be needed to obtain a more quantitative picture of these fascinating phenomena.

CONCLUSIONS

We measured the dynamics of deformation of an elastic droplet in an elastic matrix by selecting two blend systems with viscosity ratio near unity, but of different elasticities of both droplet and matrix phases. In start up of a steady shear flow, the different elasticities in the polymer blends produce qualitative differences in the droplet deformations that occur before the droplet attains its steady-state shape. In system A with higher elasticity, the deformation oscillates several times before reaching its steady-state shape. In system B with lower elasticity, the droplet first deforms in the shear direction, and thereafter continuously contacts in the flow direction until it reaches its steady-state shape. When the capillary number is increased at fixed shear rate (and hence fixed elasticity) by increasing the droplet size in system A and B, the steady-state droplet shape becomes increasingly elongated in the vorticity direction and develops cusps along the vorticity axis. In this system A, at still higher capillary number, droplet breakup occurs when two ends of a drop elongated in the vorticity direction are situated on streamlines of different velocity which pull the droplet ends apart, leading to rupture.

ACKNOWLEDGEMENTS

The authors (W.L. and A.S.) would like to acknowledge the fellowship provided by the Thailand Research Fund (TRF), Grant No. BRG/12/2544.

REFERENCES

Almusallam AS, Larson RG, Solomon MJ (2000) A constitutive model for the prediction of ellipsoidal droplet shapes and stresses in immiscible blends. J Rheol 44:1055-1083

Bartram E, Goldsmith HL, Mason SG (1975) Particle motions in non-Newtonian media. Rheol Acta 14:776-782

Branrup J, Immergut EH (1989) Polymer Handbook. 3rd Ed., New York

Bentley BJ, Leal LG (1986) An experimental investigation of drop deformation and breakup in steady, two-dimensional linear flows. J Fluid Mech 167:241-283

Grace HP (1982) Dispersion phenomena in high viscosity immiscible fluid systems and application of static mixers as dispersion devices in such systems. Chem Eng Commun 14:225-227

Graebling D, Muller R, Palierne JF (1993) Linear viscoelastic behavior of some incompatible polymer blends in the melt. Interpretation of data with a model of emulsions of viscoelastic liquids. Macromolecules 26:320-329

Guido S, Villone M (1998) Three-dimensional shape of a drop under simple shear flow. J Rheol 42:395-415

Hobbie EK and Migler KB (1999) Vorticity elongation in polymeric emulsions. Phys Rev Lett 82:5393-5396

Larson RG (1999)The structure and rheology of complex fluids. Oxford University Press, New York

Lerdwijitjarud W, Sirivat A, Larson RG (2002) Influence of elasticity on dispersed-phase droplet size in immiscible polymer blends in simple shearing flow. Polym Eng Sci 42:798-809

Lerdwijitjarud W, Larson RG, Sirivat A, Solomon MJ (2003) Influence of weak elasticity of dispersed phase on droplet behavior in sheared polybutadiene/ Poly(dimethylsiloxane) blends. J Rheol 47:37-57.

Levitt L, Macosko CW, Pearson SD (1996) Influence of normal stress difference on polymer drop deformation. Polym Eng Sci 36:1647-1655

Luciani A, Champagne MF, Utracki LA (1997) Interfacial tension coefficient from the retraction of ellipsoidal drops. J Polym Sci, Part B: Polym Phys 35:1393-1403

Mighri F, Ajji A, Carreau PJ (1997) Influence of elastic properties on drop deformation in elongational flow. J Rheol 41:1183-1201

Mighri F, Carreau PJ, Ajji A (1998) Influence of elastic properties on drop deformation and in shear flow. J Rheol 42:1477-1490

Mighri F, Huneault MA (2001) Dispersion visualization of model fluids in a transparent Couette flow cell. J Rheol 45:783-797.

Migler KB (2000) Droplet vorticity alignment on model polymer blends. J Rheol 44:277-290

Palierne JF (1990) Linear rheology of viscoelastic emulsions with interfacial tension Rheol Acta 29:204-214

Rumscheidt FD, Mason SG (1961) Particle Motions in Sheared Suspensions. XII. Deformation and burst of fluid drops in shear and hyperbolic flow. J Coll Sci 16:238-261

Taylor GI (1932) The viscosity of a fluid containing small drops of another fluid. Proc R Soc A138:41-48.

Taylor GI (1934) The formation of emulsions in definable fields of flow. Proc R Soc A146:501-523.

Tsakalos VT, Navard P, Peurel-Disdier E (1998) Deformation and breakup mechanisms of single drops during shear. J Rheol 42:1403-1417

Wu S (1987) Formation of Dispered phase in incompatible polymer blends-interfacial and rheological effects. Polym Eng Sci 27:335-343

Yamane H, Takahashi M, Hayashi R, Okamoto K (1998) Observation of deformation and recovery of poly(isobutylene) droplet in a poly(isobutylene)/poly(dimethyl siloxane) blend after application of step shear strain. J Rheol 42:567-580

TABLE

Table 1 Properties of polymer blend components

Polymer	Suppliers	Grade	Mw*	Melt Flow Index (g/10min)
PS1	Polyscience	Cat#18544	50,000	-
PS2	Polyscience	Cat#23637	800-5,000	-
HDPE1	Bangkok Polyethylene	1600J	-	14
HDPE2	Aldrich	Cat#42,801-9	-	42

* Quoted by the manufacturers

Table 2 Polymer blend systems

Blend system	Blend components (Drop/Matrix)	Temperature (°C)
A	PS1/HDPE1	147
B	PS2/HDPE2	139

FIGURE CAPTIONS

Figure 1 Viscosity η, storage modulus G', and first normal stress difference N_1 as functions of shear rate and frequency for each pure polymer at the temperatures at which the blend experiments were carried out; (a) matrix phase [HDPE1 at 147°C: η (●), G' (o), and N_1 (○), HDPE2 at 139°C: η (■) and G'(□)] and (b) droplet phase [PS1 at 147°C: η (▲), G' (△), and N_1 (△), HDPE2 at 139°C: η (◆) and G'(◇)].

Figure 2 The ratios of droplet to matrix values of the viscosity η (●), storage modulus G' (o), and first normal stress difference N_1 (▲) for (a) system A: PS1/HDPE1 at 147°C and (b) system B: PS2/HDPE2 at 139°C. These two temperatures apply to all results in the following figures for systems A and B, respectively.

Figure 3 Dependence of apparent interfacial tension value on droplet size for (a) system A and (b) system B, inferred from the Palierne formula, Eq. 4.

Figure 4 Schematic drawing of a single drop observed from the "side" and "top" views by optical microscopy, a and b: the long and short axes of the droplet in the flow-gradient plane, a*: the a axis projected into the flow direction and c: the principal axis in the radial direction.

Figure 5 The time-dependent deformation of 75 (±10%)μm-drops after startup of steady shear at a rate, 0.5 s^{-1}, for system A. (a) Def* vs. time on a log time scale, (b) Def* vs. time on a linear time scale, (c) a^*/D_o vs. time on a log time scale, and (d) c/D_o vs. time on a log time scale. [initial droplet sizes (μm): 76 (●), 68 (⊙), 74 (▼), 69 (▽), 71 (■), 85 (⊡), 76 (◆), 75 (◈), 74 (▲), 70 (◬), and 79 (⬢)]

Figure 6 Sequence of images of deformed droplets of initial radius 75 (±10%) μm-after startup of a steady shear at a rate of 0.5 s^{-1} for system A; (a)-(f) images of different droplets with lens magnification of 20x [D_o = 69, 69, 71, 76, 75, and 74 μm, respectively]; (g)-(p) images of a single droplet with the lens magnification of 4x [D_o = 79 μm].

Figure 7 Schematic drawing of droplet rotation in the flow-gradient plane.

Figure 8 Sketch of a steady-state deformed droplet.

Figure 9 Time-dependent deformation of a 204 μm-droplet under constant shear rate, 0.4 s^{-1}, for system B.

Figure 10 Time-dependent droplet deformation at different values of Ca, controlled by changing the droplet diameter D_o [D_o = 52 μm; Ca = 5 (●), D_o = 79 μm; Ca = 8 (o), D_o = 110 μm; Ca = 11 (▼), D_o = 120 μm; Ca = 12 (▽)] at the same shear rate 0.5 s^{-1} (and therefore the same elasticity) for system A: (a) Def*, (b) a^*/D_o, and (c) c/D_o.

Figure 11 Time-dependent droplet deformation at different shear rates (and therefore different elasticities), at a capillary number Ca of 8, held fixed by varying by varying the initial droplet diameter inversely with the shear rate for system A: (a) Def* vs time, (b) a^*/D_o vs time, and (c) c/D_o vs time. Three different shear rates were used. (1): $\dot{\gamma}$ = 0.28 s^{-1}, with D_o = 135 μm (▲) and a repeat run at this shear rate with the same droplet size, D_o = 135 μm (△)]. (2): $\dot{\gamma}$ = 0.5 s^{-1}: D_o = 70 μm (●), and a repeat run with a slightly larger droplet, D_o = 79 μm (o). (3) $\dot{\gamma}$ = 0.8 s^{-1}, D_o = 45 μm (■)].

Figure 12 Dependence of steady-state deformation parameter on Ca for system A: shear rate 0.3 s^{-1} (○), shear rate 0.5 s^{-1} (▲), and for system B: shear rate 1 s^{-1} (□)].

Figure 13 Sequence of images during droplet breakup in system A, D_o= 120 μm, at a shear rate of 0.5 s^{-1} (Ca=12). The flow direction is horizontal, and the vorticity direction vertical.

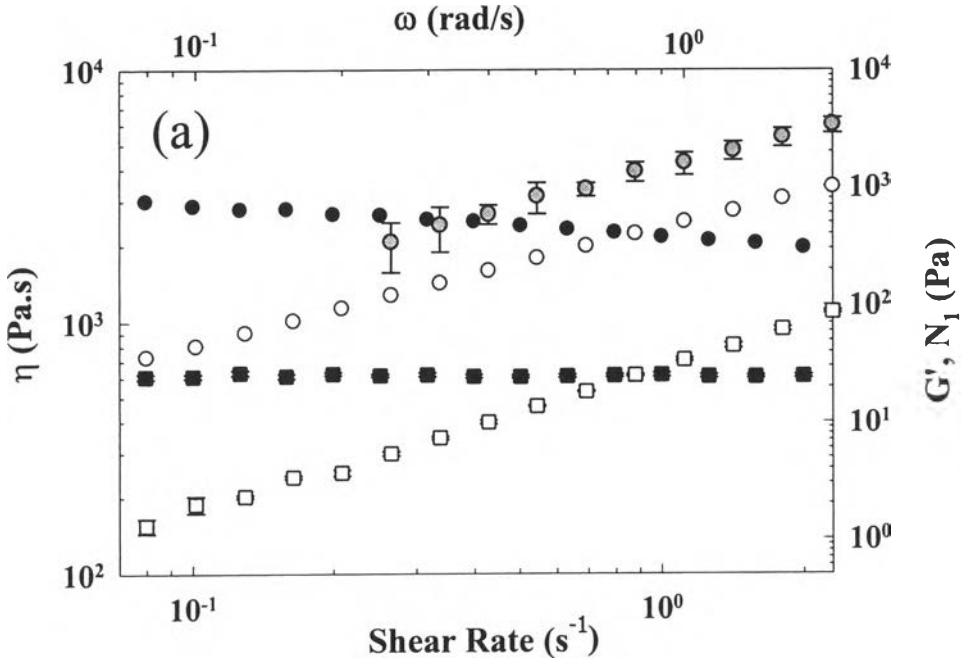

Figure 1 (a)

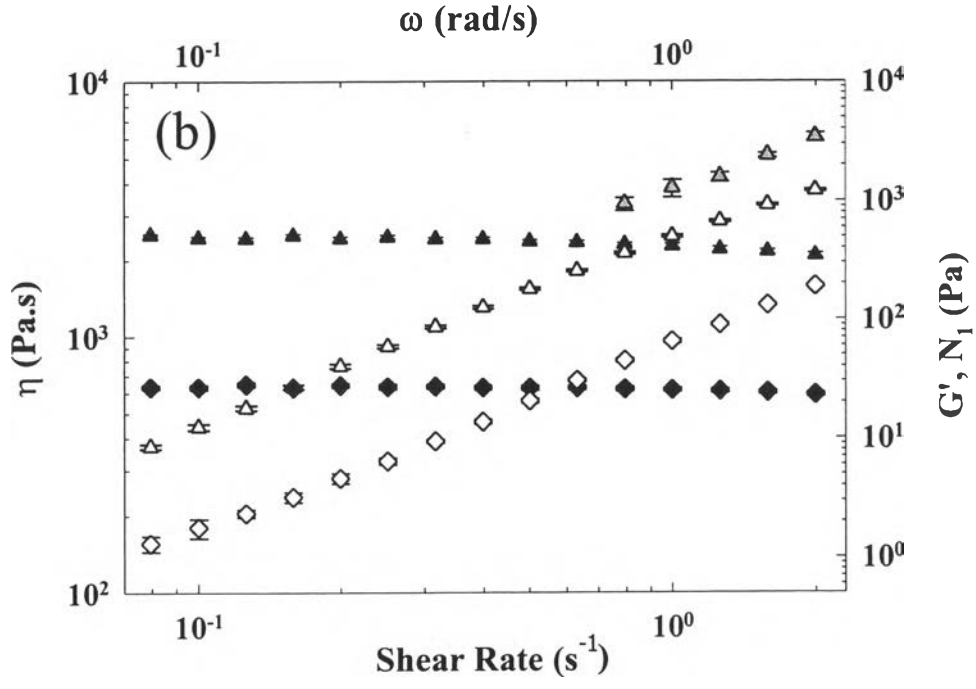

Figure 1 (b)

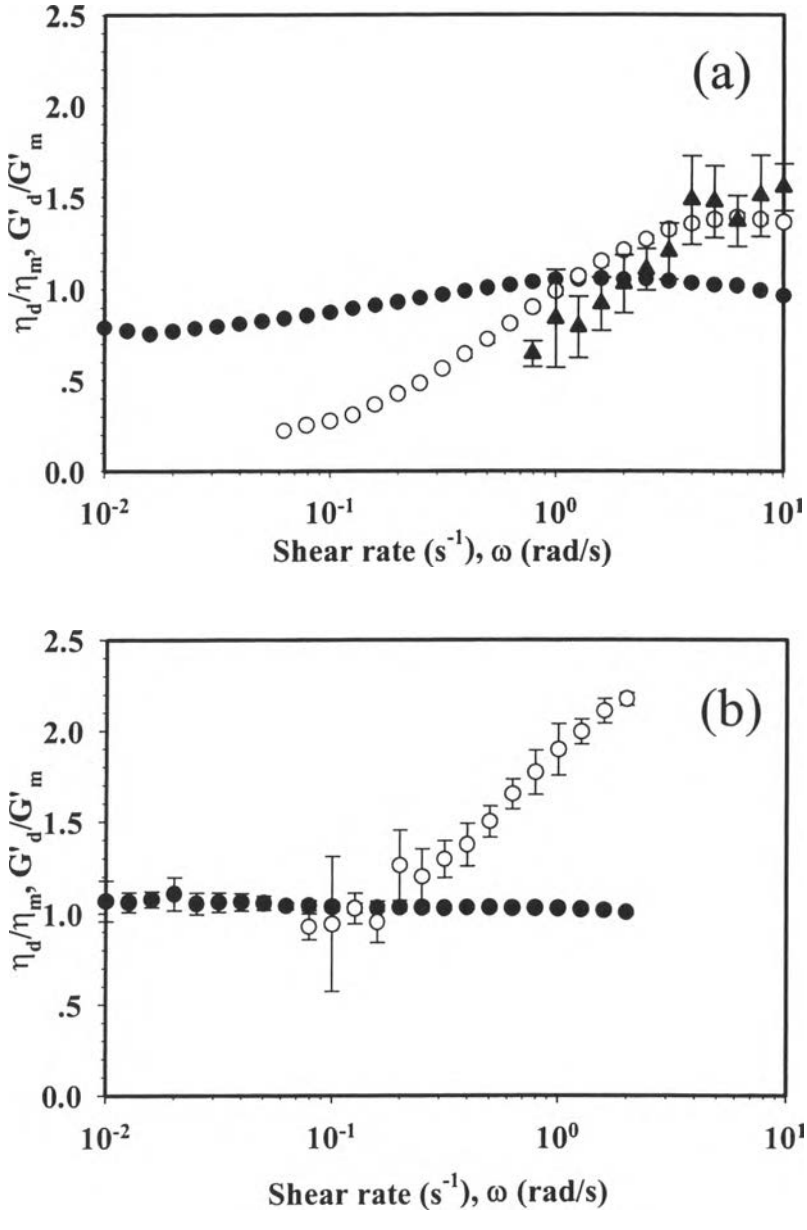

Figure 2 (a) and (b)

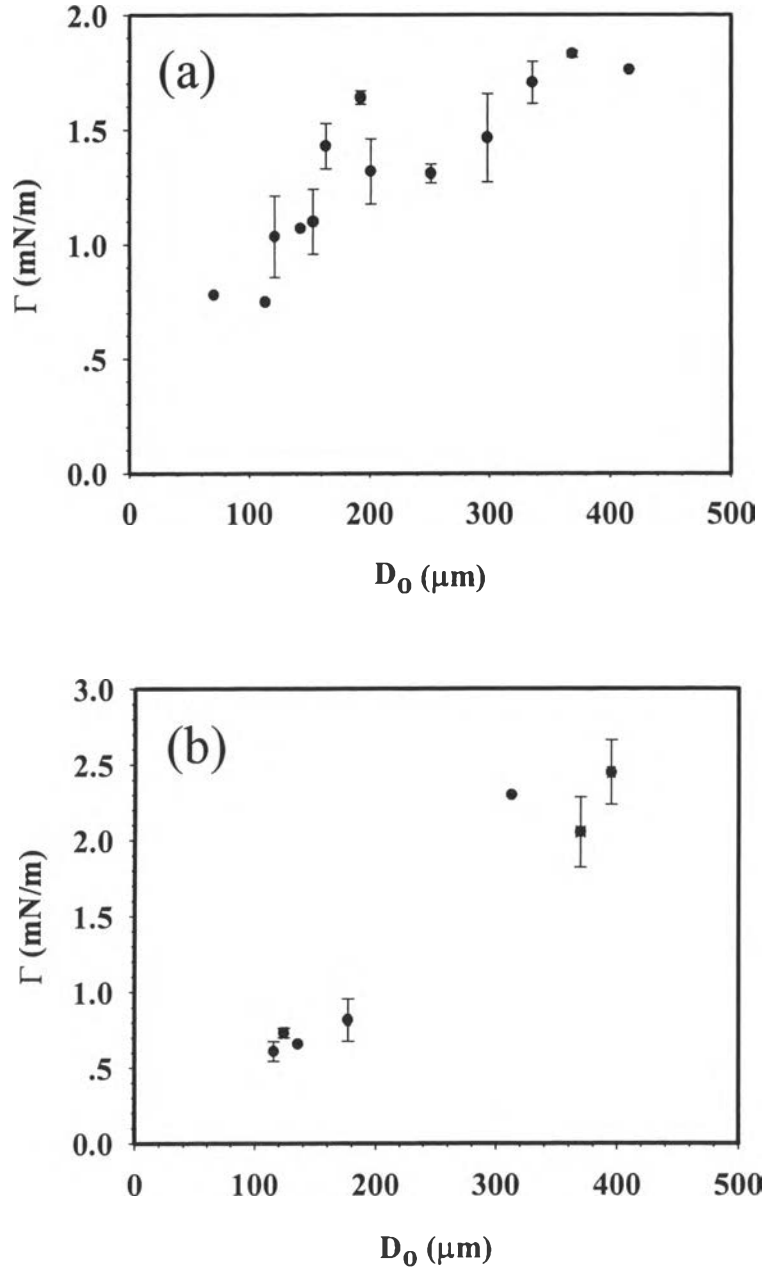

Figure 3 (a) and (b)

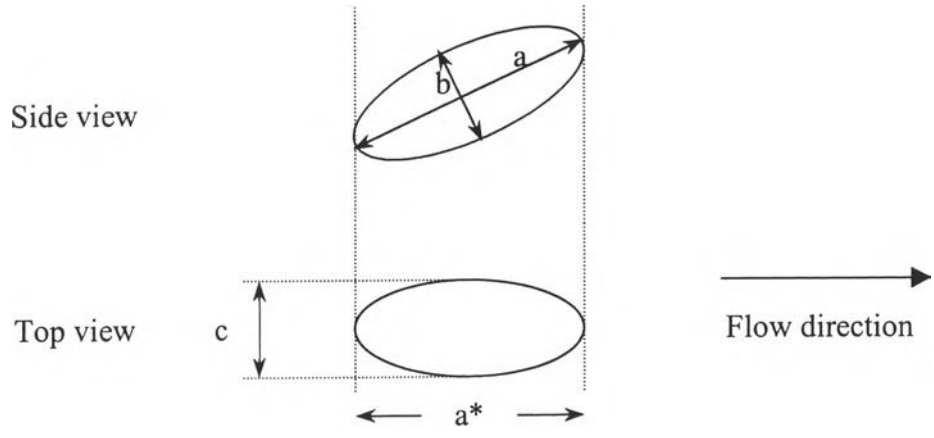

Figure 4

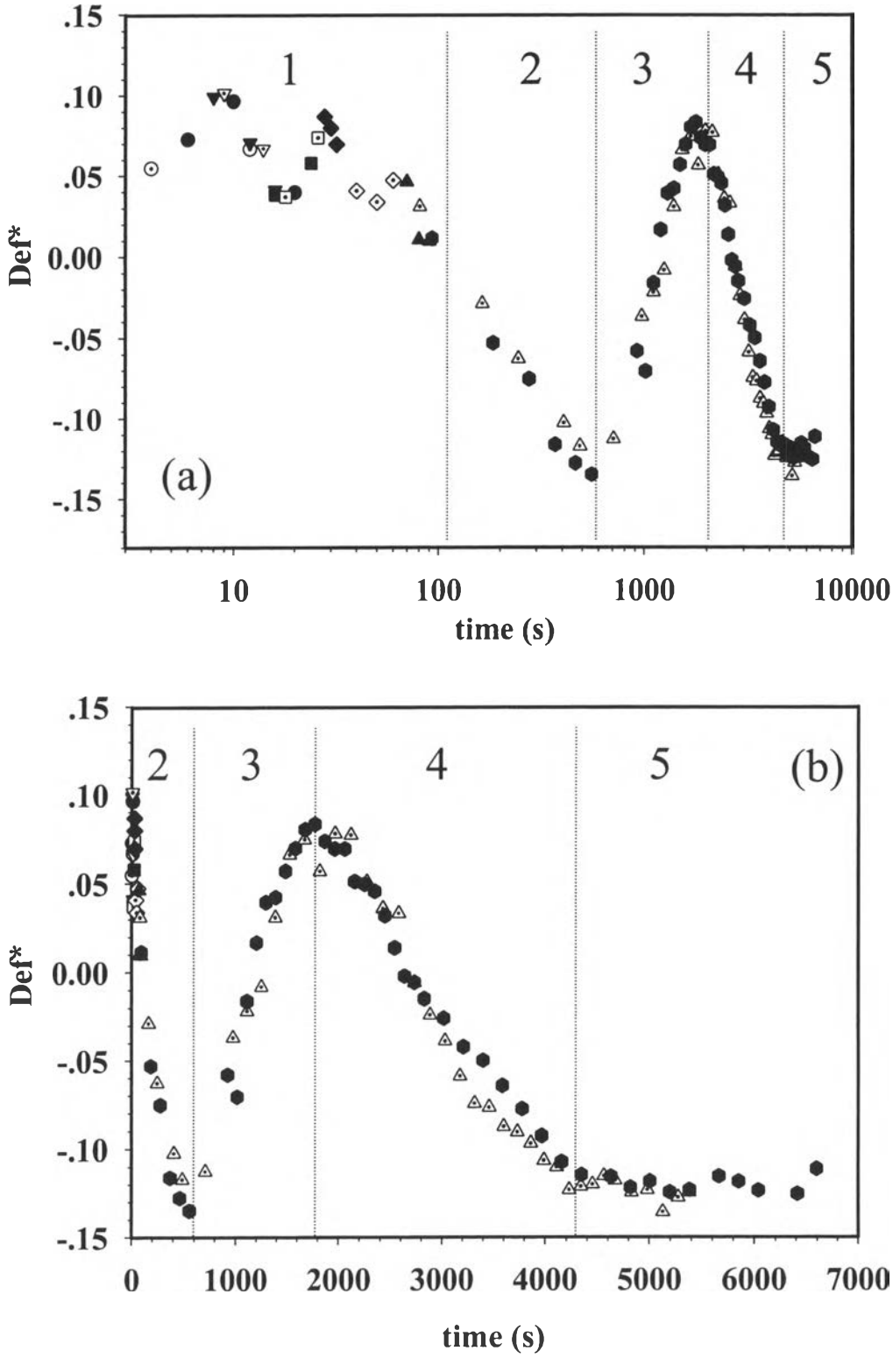
.15
.10
.05
0.00
-.05
-.10
-.15
Def*
1
2
3
4
5
(a)
10
100
1000
10000
time (s)
2
3
4
5
(b)
0
1000
2000
3000
4000
5000
6000
7000
time (s)

Figure 5 (a), (b)

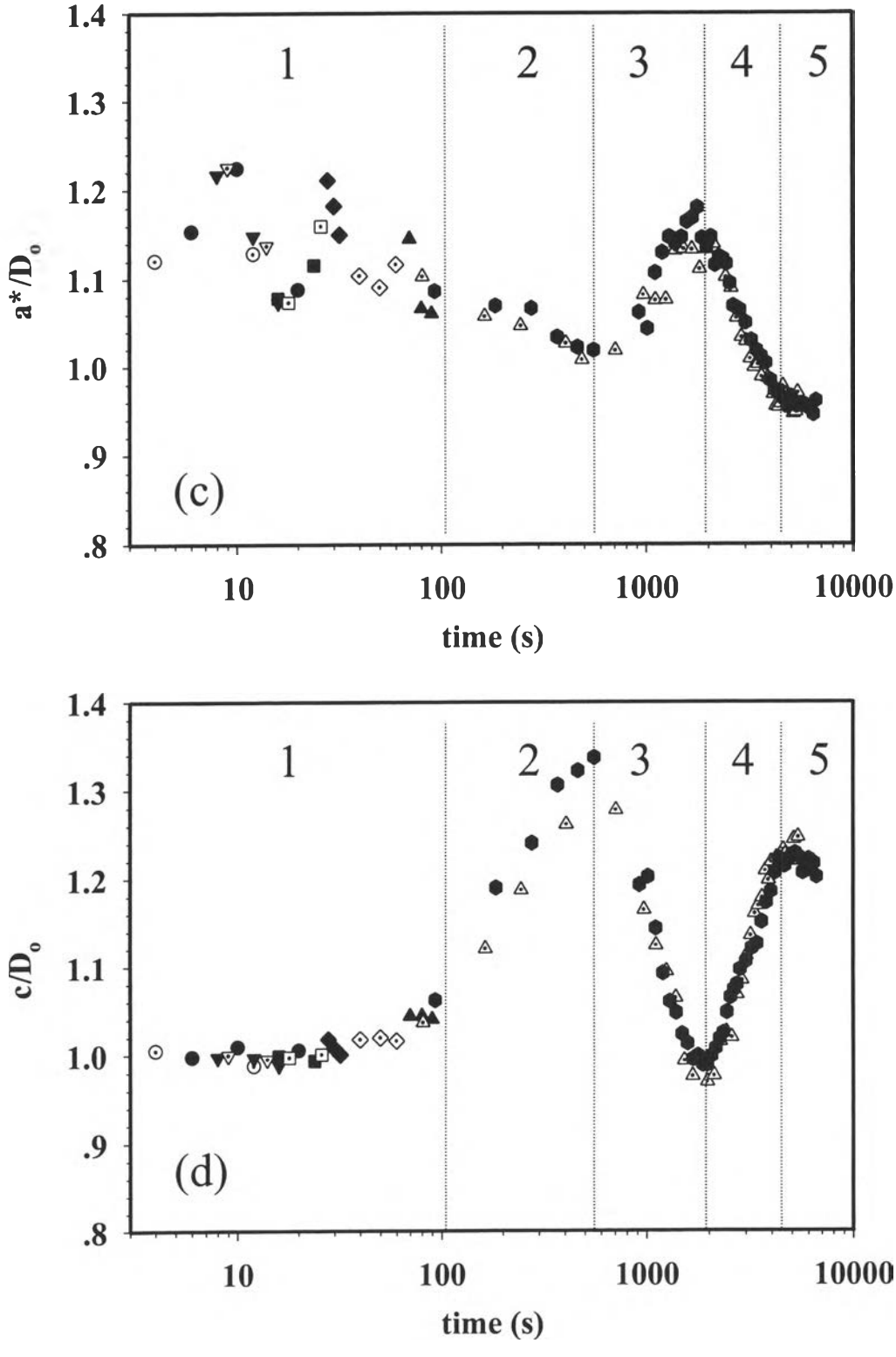
1.4
1.3
1.2
1.1
1.0
.9
.8
a*/D$_o$
1
2
3
4
5
(c)
10
100
1000
10000
time (s)
1.4
1.3
1.2
1.1
1.0
.9
.8
c/D$_o$
1
2
3
4
5
(d)
10
100
1000
10000
time (s)

Figure 5 (c), (d)

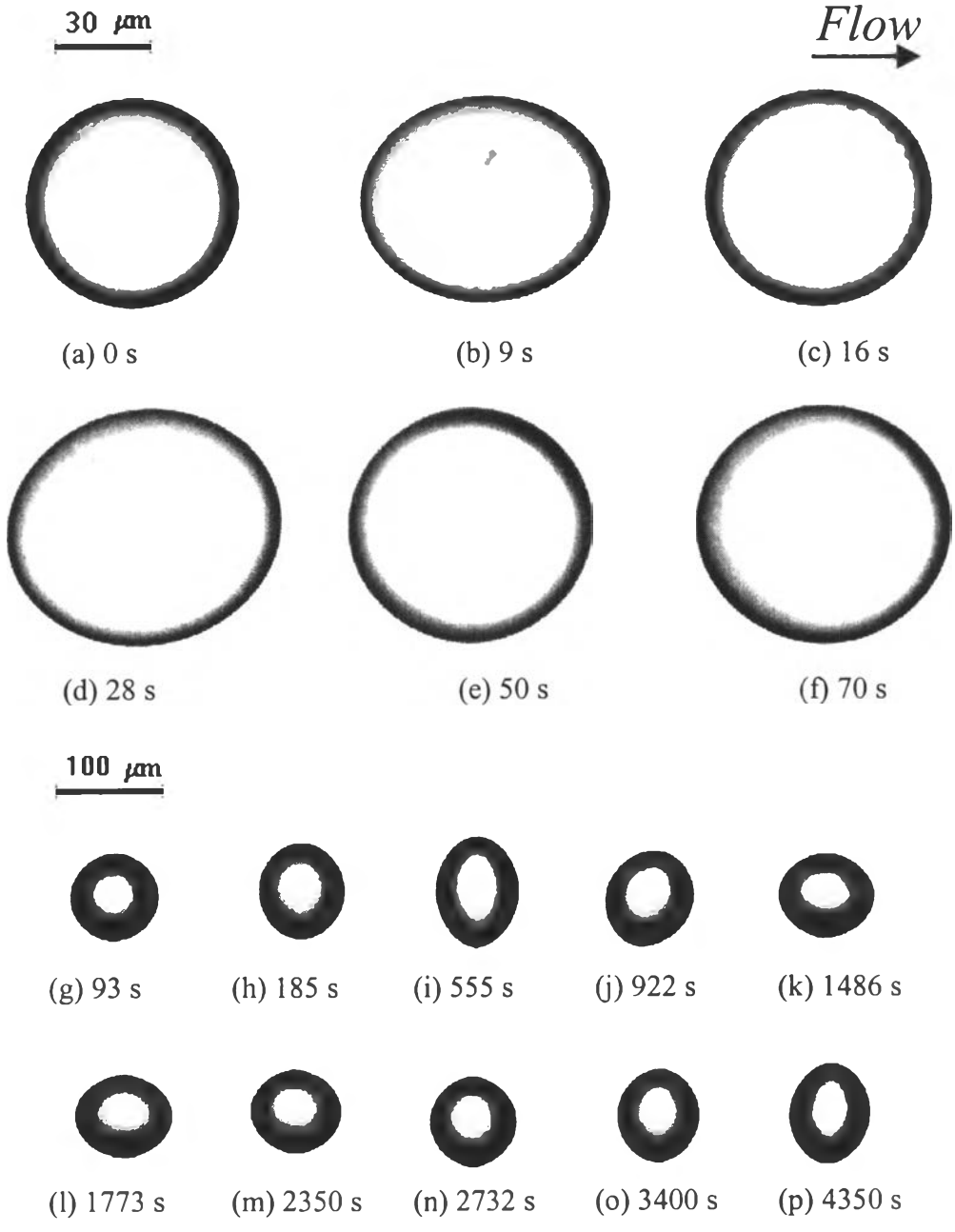
30 μm
Flow
(a) 0 s
(b) 9 s
(c) 16 s
(d) 28 s
(e) 50 s
(f) 70 s
100 μm
(g) 93 s
(h) 185 s
(i) 555 s
(j) 922 s
(k) 1486 s
(l) 1773 s
(m) 2350 s
(n) 2732 s
(o) 3400 s
(p) 4350 s

Figure 6

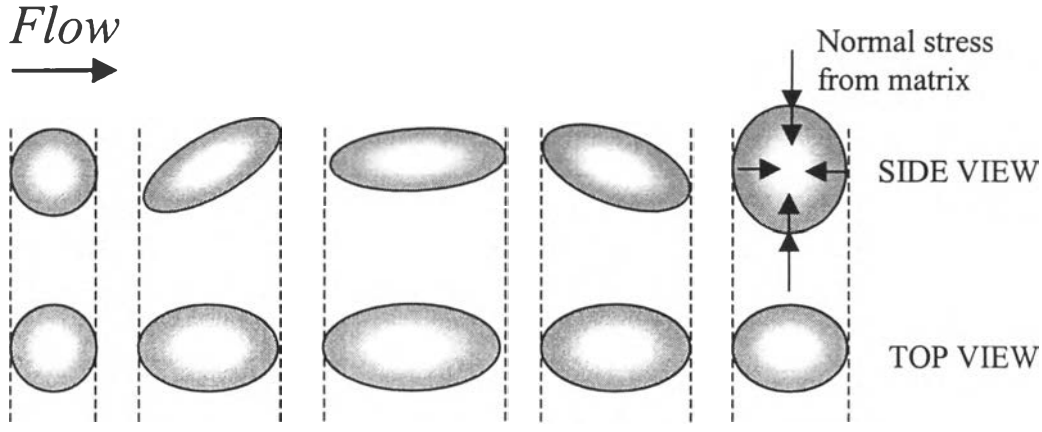

Figure7

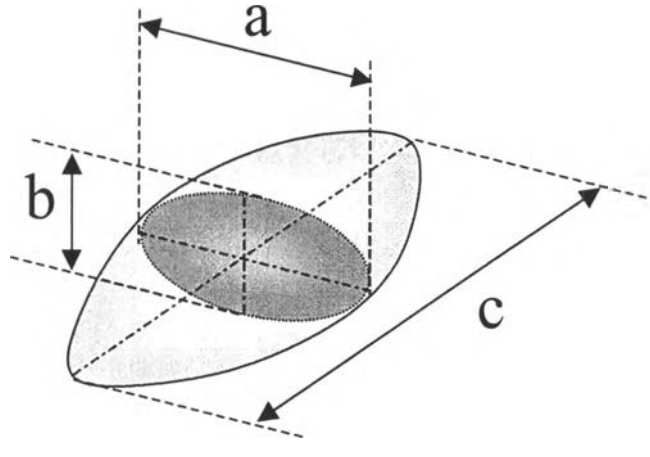

Figure 8

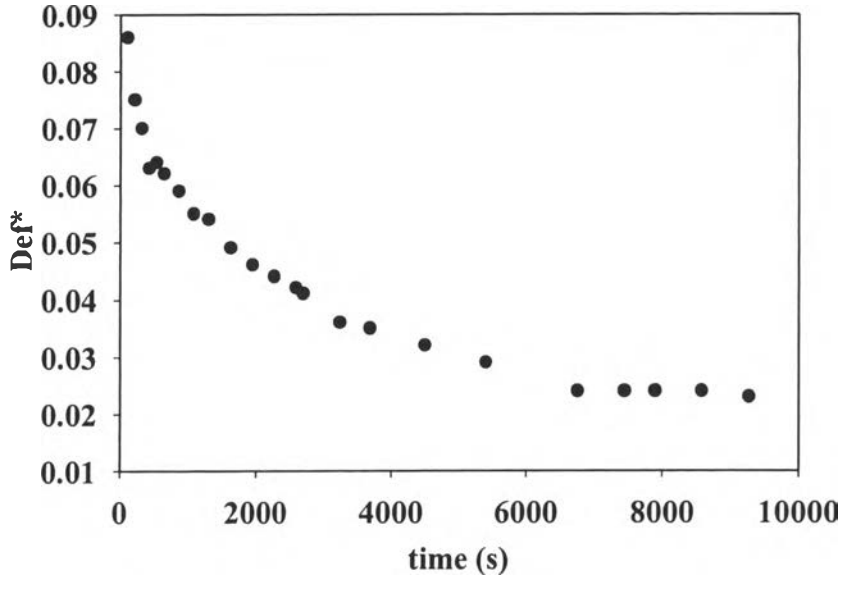
0.09
0.08
0.07
0.06
0.05
0.04
0.03
0.02
0.01
Def*
0
2000
4000
6000
8000
10000
time (s)

Figure 9

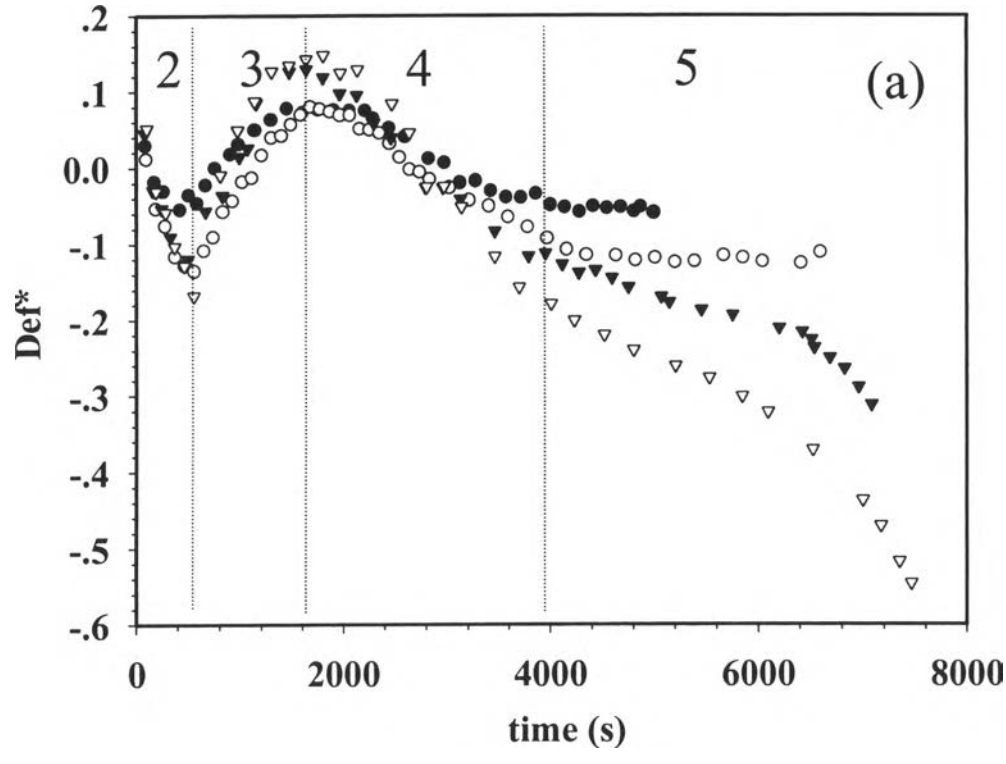

Figure 10 (a)

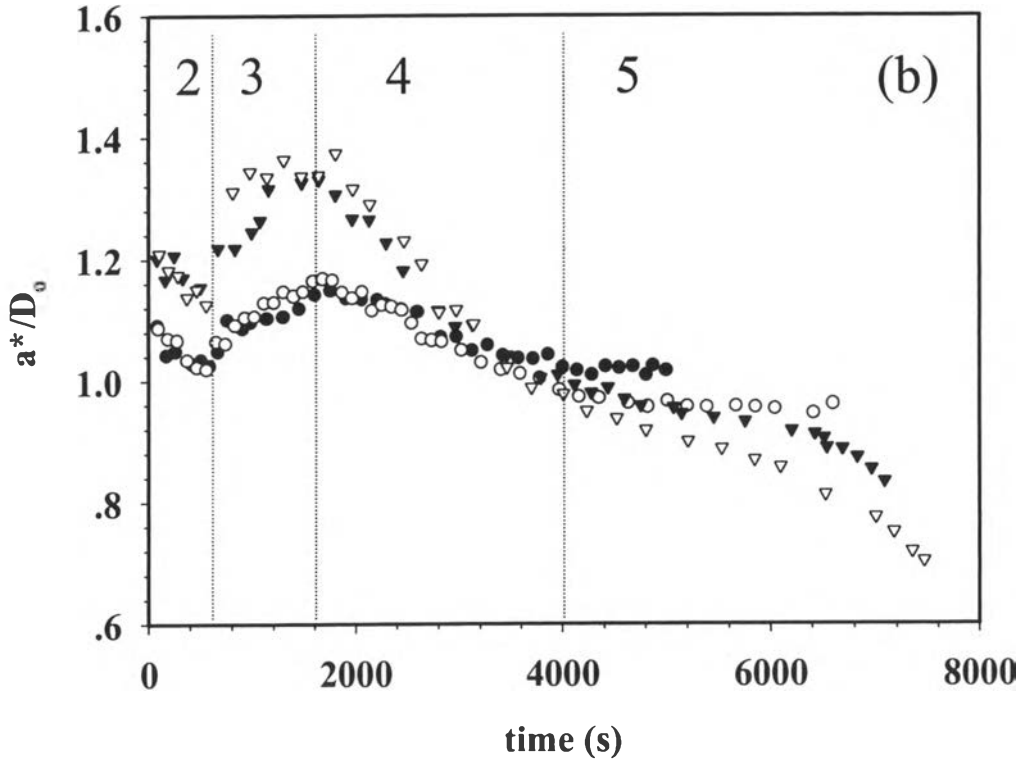
1.6
1.4
1.2
1.0
.8
.6
a*/D0
2
3
4
5
(b)
0
2000
4000
6000
8000
time (s)

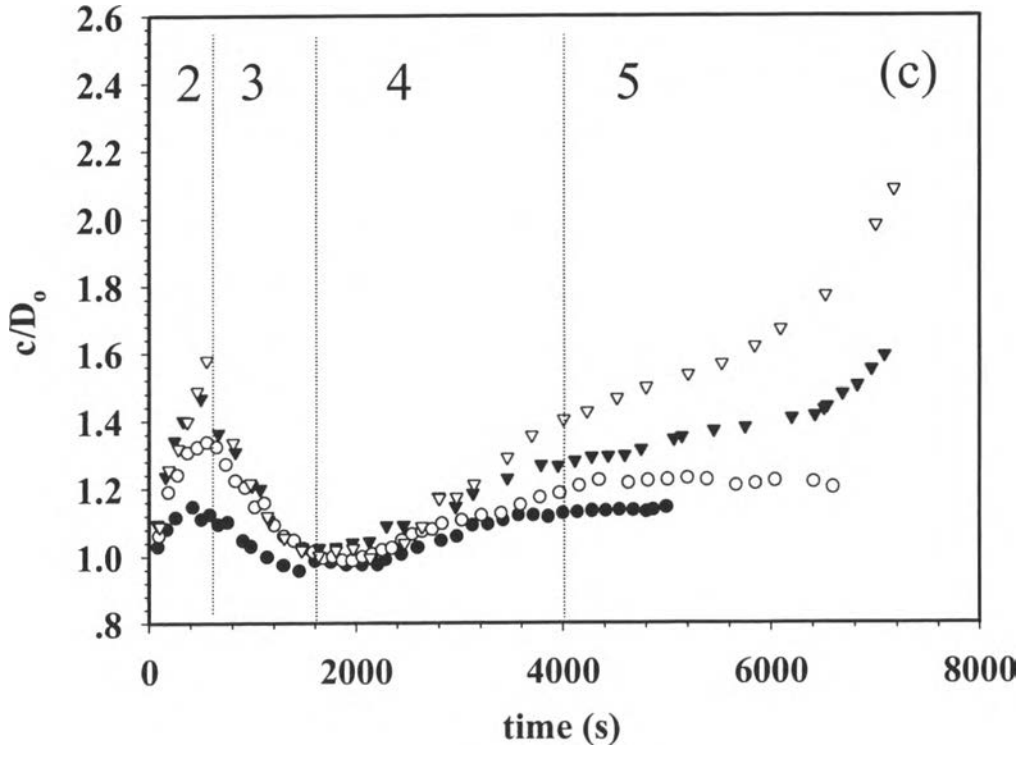
2.6
2.4
2.2
2.0
1.8
1.6
1.4
1.2
1.0
.8
c/D0
2
3
4
5
(c)
0
2000
4000
6000
8000
time (s)

Figure 10 (b), (c)

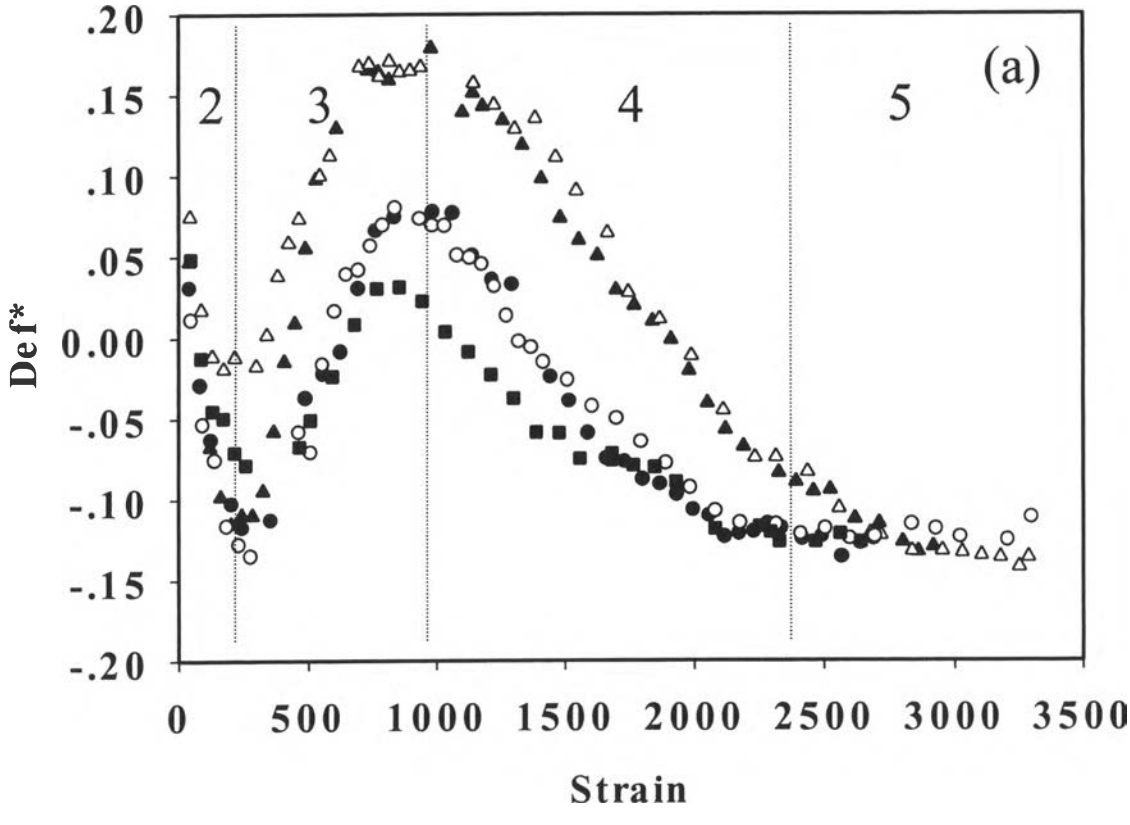
.20
.15
.10
.05
0.00
-.05
-.10
-.15
-.20
Def*
2
3
4
5
(a)
0
500
1000
1500
2000
2500
3000
3500
Strain

Figure 11 (a)

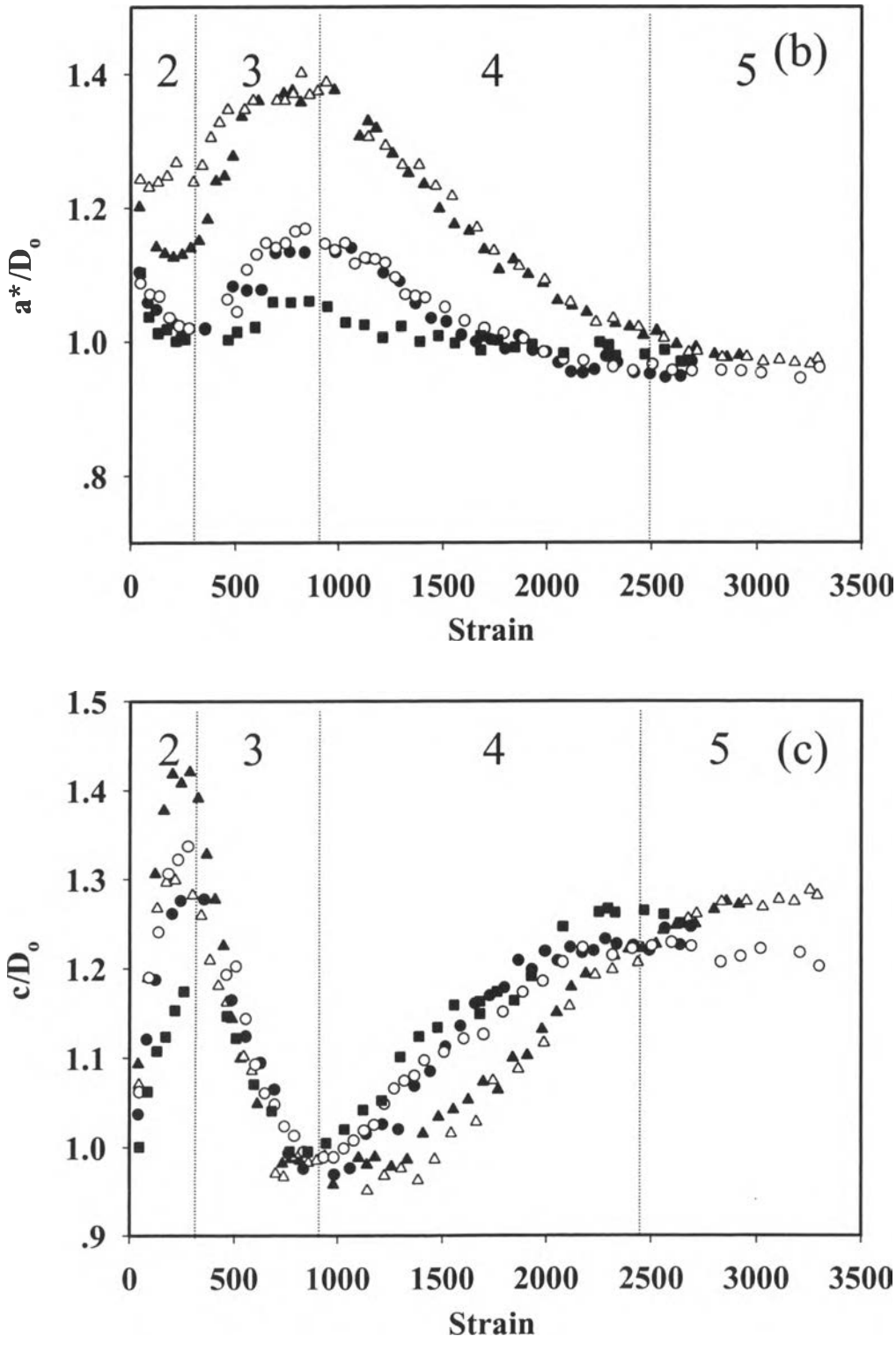
2
3
4
5
(b)
1.4
1.2
1.0
.8
a*/D$_o$
0
500
1000
1500
2000
2500
3000
3500
Strain
2
3
4
5
(c)
1.5
1.4
1.3
1.2
1.1
1.0
.9
c/D$_o$
0
500
1000
1500
2000
2500
3000
3500
Strain

Figure 11 (b), (c)

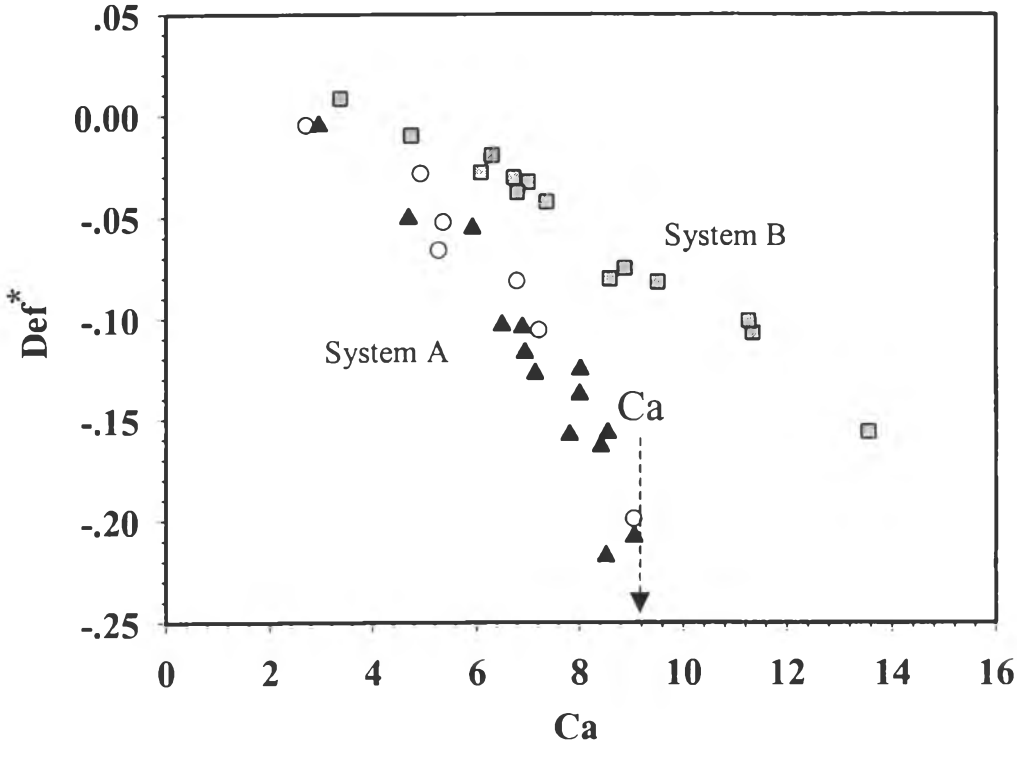

Figure 12

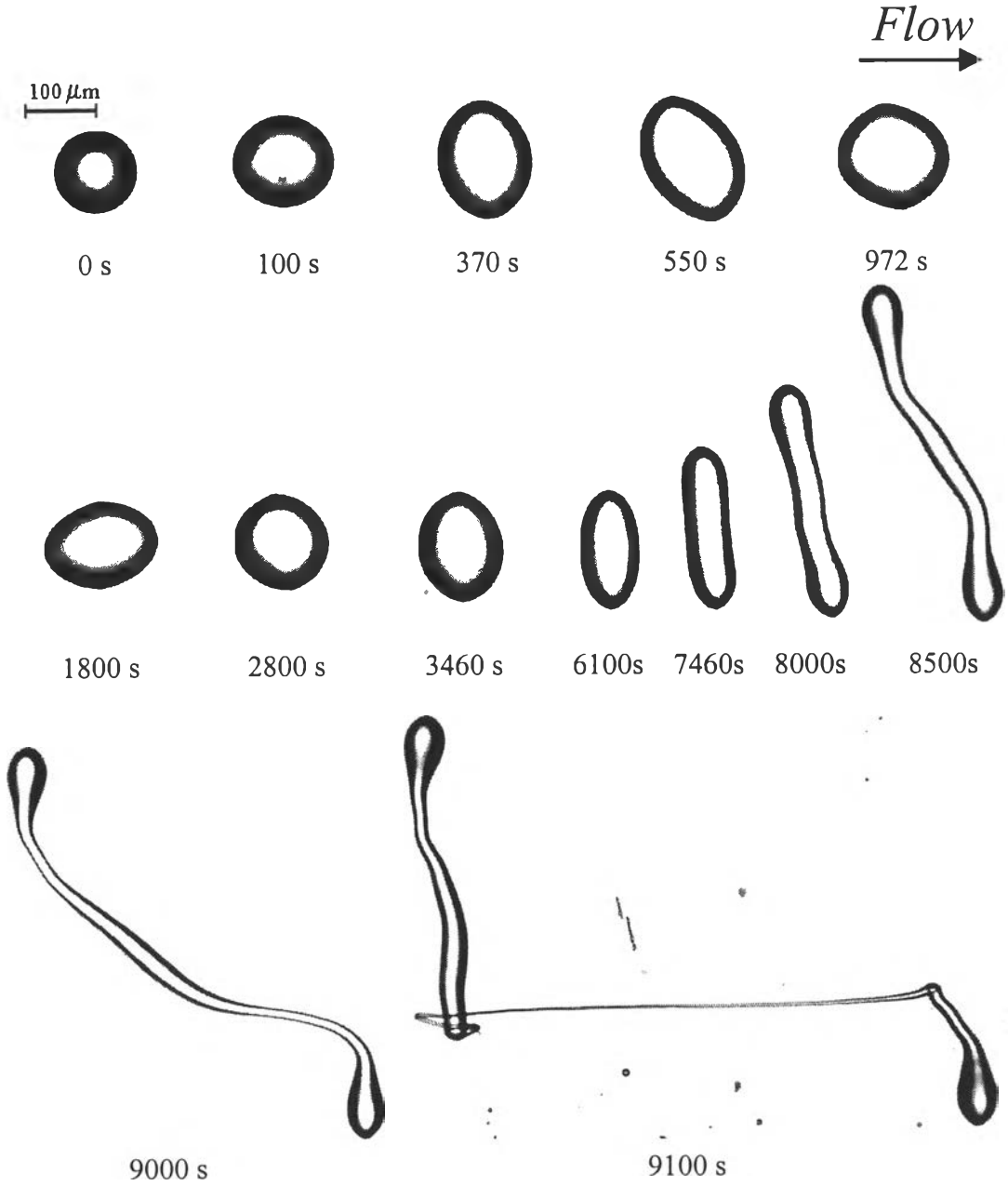
Flow
100 μm
0 s
100 s
370 s
550 s
972 s
1800 s
2800 s
3460 s
6100s
7460s
8000s
8500s
9000 s
9100 s

Figure 13